J. Fluid Mech. (1973), *vol.* 57, *part* 1, *pp.* 177–208
Printed in Great Britain

Flow of dilute polymer solutions about circular cylinders

By TURGUT SARPKAYA, P. G. RAINEY† AND R. E. KELL‡
Naval Postgraduate School, Monterey, California

(Received 24 March 1972 and in revised form 4 September 1972)

Experiments on fully attached flows of aqueous solutions of Polyox WSR-301 and pure solvent (tap and distilled water) about circular cylinders were carried out in the range $5 \times 10^4 < Re < 3 \times 10^5$ for the initial purpose of providing definitive experimental information on drag reduction with additives in external flows.

During the course of the investigation, a critically degraded polymer solution was observed to cause, at a particular Re, an unforseen instability in the separation line, similar to that first observed by Brennen (1970) in fully developed cavity flows. This instability, which most easily manifested itself in the form of an abrupt drag-force jump (here called a drag crisis) from a high subcritical to a low supercritical value, became the central issue in the investigation. Efforts to isolate the causes of this instability led to further experiments with suspensions of nearly neutrally buoyant spherical and non-spherical particles. The measurements have shown that fibres and polymer hasten transition, spherical particles do not appreciably affect the characteristics of the flow and that neither the spherical particles nor fibres give rise to a drag crisis.

1. Introduction

The reduction of resistance to turbulent shear flows of liquids through the addition of fibres and in particular small quantities of polymers of high molecular weight has received considerable attention. The research efforts and results available in this field have been reviewed and summarized from several points of view (e.g. Hoyt 1968, 1972; Lumley 1969). Although extensive theoretical and experimental work has been carried out with steady pipe flows (e.g. Virk 1971; Bryson, Arunachalam & Fulfords 1971; Kerekes & Douglas 1972), where the resistance is due to turbulent skin friction alone, relatively few studies have been conducted on the effect of additives on the flow about bluff bodies.

The earliest known experiment with bluff bodies in drag-reducing polymers was carried out by Crawford & Pruitt (1963). Additional experiments with different sizes and shapes of bodies (mostly spheres and cylinders) in various types and concentrations of polymers were conducted by others (e.g. Rusczycky 1965; Barenblatt, Bulina & Myasnikov 1965; Merrill, Smith, Shin & Mickley 1966; Merrill, Smith & Chung 1966; A. White 1966, 1967; D. A. White 1966;

† Present address: Boston Naval Shipyard, Boston, Mass.
‡ Present address: Philadelphia Naval Shipyard, Philadelphia, Penn.

Gadd 1966; Hayes 1966; Lang & Patrick 1967; Chenard 1967; James 1967; Sanders 1967; McClanahan & Ridgely 1968; Luikov, Shulman & Puris 1969; James & Acosta 1970; Brennen 1970; Kalashnikov & Kudin 1970; Sarpkaya & Rainey 1971). An annotated catalogue of these investigations has recently been presented by Sarpkaya, Rainey & Kell (1972). Here only those studies which have a direct bearing on the present work will be briefly described.

Brennen (1970) investigated the effect of several types of polymer additives in flows with ventilated cavities, in the subcritical range $10^4 < Re < 8 \times 10^4$, on the position of the separation line on two spheres and a circular cylinder. His motion pictures have shown that the separation line on the spheres moved downstream from its position for water and that there was no significant separation shift on the particular cylinder used. Even more significant, however, was Brennen's observation of a particular type of instability which the additive caused in the wetted surface flow around the headform: after a certain speed (7 ft/s for 0·5 in. sphere and 8 ft/s for the 0·25 in. cylinder) the separation line became gradually distorted into a wavy pattern. Degradation produced no measurable effect on the magnitude of the spanwise wavelength exhibited at a particular speed and slightly increased the critical speeds at which the various types of distortion occurred. However, even for the most degraded solution, these threshold speeds were not raised by more than about 3 ft/s.

In an effort to explain his observations, Brennen suggested that elastic energy is stored in additive molecules or micelle structure in their respective 'effective regimes' and then released in the steady or retarded region of the flow, leading to the rapid growth of the unstable disturbances, separation-line distortion etc.

Luikov *et al.* (1969) carried out experiments with sodium carboxymethylcellulose solutions at high concentrations and found that the separation point moved farther downstream. They conjectured that the decrease of the resistance of the cylinder was partly due to the smaller size of the wake and partly due to a change in the character of the vortical motion behind the cylinder. A similar study by Barenblatt *et al.* (1965) with rough cylinders and dilute-polymer or glycerine injection at suitable points has shown that the contraction of the wake and the displacement of the separation point farther downstream cannot conclusively explain the drag-reduction phenomenon in external flows.

Several facts emerge from the foregoing and other studies cited earlier: (*a*) the mechanisms responsible for drag reduction are still not understood; (*b*) apart from the inherent complexities of the phenomenon, the difficulties with external flows are added to the many factors which affect separation, transition, and the characteristics of the near-wake flow; and finally (*c*) the research efforts, including the present one, reflect only indirectly the mechanism(s) by which additives affect drag reduction. In other words, there is continued need for definitive experimental information in the light of which the mechanisms proposed may be scrutinized and appropriate analytical models may be developed. It was with this objective that the present investigation was undertaken.

Our results consist of measurements, simultaneously or in groups, of drag, pressure distribution, vortex-shedding frequency, separation angle, turbulence intensity of the ambient and wake flow, and some measure of degradation or the

friction-reducing effectiveness of the solution. The data were compared with similar data obtained with pure solvent and with suspensions of nearly neutrally buoyant spherical and non-spherical particles in water.

In examining the relation between *Re*, the polymer-solution and fibre suspension characteristics and the drag crisis, several questions have been treated. First, and most essential, how do the drag coefficient, pressure distribution, Strouhal frequency, flow separation, etc., evolve with degradation? Second, how do these same parameters return to their independently measured, pure-solvent values as the polymer continues to degrade further beyond a critical value measured in terms of the friction-reducing effectiveness of the solution? Third, how do the measurements made in polymer-solution and pure-solvent flow compare with those made in suspension flow? Finally, an attempt is made to interpret the results in the light of the previously proposed drag-reduction mechanisms. The first three matters are reports on new data; the fourth is more speculative.

The results appear to favour one of the earlier notions that entanglement or aggregation of polymer molecules could be one of the important mechanisms in drag reduction and that a suitable model should consider a non-continuum medium in which the visco–inertial action of the deformable particles affects the surrounding fluid.

2. Apparatus and experimental procedure

2.1. *Water tunnels*

The first series of experiments was performed in a recirculating water tunnel (hereafter referred to as the NPS tunnel) of approximately 500 gallons capacity equipped with a perspex test section 4 in. wide, 8 in. high and 26 in. long (Sarpkaya & Rainey 1971). Evidently, the width of this test section was somewhat small relative to the particular size of the test bodies (0·5–1·5 in. diameter) which had to be used to reach the critical-transition range in pure-solvent flow. The data obtained from these experiments, however they may have been affected by the particular length-to-diameter ratios of the cylinders used, served to uncover all the basic features of the phenomenon and in particular the aforementioned instability, and to define the central issues of the investigation. The second series of experiments was conducted by the senior author in the larger Göttingen tunnel (Aerodynamische Versuchsanstalt-Göttingen), which is equipped with a clear plastic test section 50 in. long, 9·84 in. wide and 13·8 in. high, for the express purposes of verifying the accuracy of the first series of tests and of ascertaining that the observed drag crisis was not a peculiar manifestation of the tunnel and the test conditions used. In both tunnels, a continuously variable speed motor and pump combination circulated the fluid at test-section velocities ranging from 4 ft/s to approximately 30 ft/s. Screens were not used, to minimize polymer degradation, but properly streamlined contractions and a number of flow straighteners were placed upstream of the test sections. These proved sufficient to provide velocity profiles which remained uniform within a region of 0·2 in. away from the top and bottom of the test sections with a standard deviation of 1·8 %. The

free-stream turbulence level $(\overline{u^2})^{\frac{1}{2}}/U$ was found by hot-film anemometer techniques (using a conical probe and the associated equipment described in §2.3) to be 1–2 % throughout the range of the test-section velocities.

2.2. *Test cylinders*

Aluminium cylinders of diameter 0·75 in., 1 in., 1.5 in. and 1·97 in., placed across the width of the test section, were used for direct drag measurements. One end of each cylinder was held by a self-aligning bearing imbedded in one perspex window. The other end passed through the opposite window and was connected to a waterproofed, vertically mounted, cantilever beam fitted with a strain gauge. An instrument box, filled with water through the 0.04 in. clearance between the cylinder and the perspex window, housed the cantilever-beam system and the other devices for measuring forces directly.

Perspex cylinders 0·5 in., 1 in. and 1·97 in. in diameter, extending through both tunnel walls, i.e. with no gap between the cylinders and the tunnel walls, were used for pressure measurements and flow visualization. They were externally fitted with O-rings which permitted rotation to any desired angle, yet completely sealed the passage through the perspex walls. A small-bore hole at the centre-plane served as the total pressure tap. Static pressure taps were placed near the entrance to the test section. Additional radial holes were drilled along these cylinders to allow dye to be injected into the free stream to facilitate flow visualization. Still photographs as well as a number of high-speed cine films of the dye filaments in the vicinity of the separation line were made.

The local static pressure on the cylinder surface was measured at 5° intervals around the circumference at the centre-plane. The pressure-drag coefficient was calculated from the pressure distribution for comparison with that obtained from the direct drag measurements.

Perspex cylinders of diameter 1 in. and 1·5 in., mounted as just described above, were used for the shedding-frequency studies in a manner similar to that used by Drescher (1956) and Bublitz (1971). Fluctuating pressure and local pressure measurements were made on the surface of the cylinder through a small-bore hole drilled radially from the cylinder surface and leading to a larger hole drilled axially from the cylinder end. Small brass tubes were tapped into the end holes to be used as pressure taps. Each cylinder had three small-bore holes at 0°, 135° and 225° located in the centre-plane.

An aluminium cylinder of 1 in. diameter was used for the combined frequency–drag studies and was mounted in a manner similar to that used for the direct drag measurements. This mirror-polished cylinder contained two pressure taps drilled radially at 0 ° and 120° from the forward stagnation point for stagnation and fluctuating pressure measurements respectively. Two larger axially drilled holes were mounted with brass tubes for pressure tapping. Then two, short, soft polygon tubes, which did not affect the drag measurements, connected these pressure taps to two stationary taps on the outer face of the tunnel window. The latter were in turn connected to various types of commercially available pressure transducers. A detailed description of this apparatus is presented elsewhere (Akad 1969; Hendricks 1970; Sarpkaya & Rainey 1971; Kell 1971).

2.3. *Instrumentation*

The instantaneous value of the drag force acting on the cylinders was directly measured with cantilever beam fitted with a strain gauge. The Strouhal frequency data for 1 in. and 1·5 in. perspex cylinders were calculated from fluctuating pressure measurements taken at two points, located directly opposite each other at $\pm 45°$ from the rear stagnation point. The two pressure leads of equal length were attached to a differential pressure transducer with a rated high frequency response of 1500 Hz. The output of the transducer was fed into a multi-channel amplifier-recorder system. A suitable counter was added to the output of the carrier amplifier to check the data. The counter results agreed exactly with those of the chart recorder.

Frequency spectrum measurements were made using only one tap at 60° from the rear stagnation point instead of two taps at $\pm 45°$. Initial checks were made in both polymer and water to determine the point on the downstream face of the cylinder where the maximum pressure signal (absolute value) occurred. In water, this point was located at approximately 125° from the forward stagnation point. In a 25 p.p.m. solution of polymer the maximum pressure occurred at 110°. A single point at 120° was chosen for all tests since the readings at this point in polymer solution and water were less than 1 % below the maximum. Additional details of the instrumentation and procedure are presented in Kell (1971).

Exploratory measurements were made (in flows of water and polymer solutions only) with a conical hot-film probe of the turbulence intensity, microscale of turbulence (Hinze 1959), frequency spectrum and the wake width in the near-wake flow field of a 1 in. perspex cylinder using conventional constant-temperature hot-wire anemometry. Microscale measurements were obtained by feeding the bridge-output signal of the anemometer to a sum and difference differentiator unit, from which the time derivative of the sensor signal was obtained. This signal was fed to an r.m.s. meter, and to an amplifier with a low and high cut-off of 0·1 and 1·000 Hz, respectively.

Frequency spectrum measurements were made by band passing the taped hot-film sensor signal through a band-pass filter. The filtered signal was fed to an r.m.s. voltmeter with a time constant of 3 s. A schematic diagram of the electronic system and the complete details of the measurements are available elsewhere (Kell 1971; Schimmels 1971).

2.4. *Polymer and its mixing*

The polymer used in all the experiments reported here was Polyox WSR-301, a straight-chain polyoxyethylene manufactured by the Union Carbide Corporation. The steady-state intrinsic viscosity of the fresh solution, measured by a Well–Brookfield micro-viscometer, was 16·1 dl/g. The weight-average molecular weight and the radius of gyration, calculated from the relationships derived by Merrill, Smith, Shin & Mickley (1966) and Merrill, Smith & Chung (1966), were $4{\cdot}6 \times 10^6$ and 2200 Å respectively.

During the first two years of the investigation, the polymer solutions were

prepared by mixing the dry polymer powder in distilled water to a concentration of 1000 p.p.m. (Akad 1969; Hendricks 1970). After being stirred gently for about an hour, the solution was introduced into the deaerated and filtered water in the tunnel in the amounts desired while the main pump ran at its lowest speed. Then the solution was aged for approximately 24 h. The cylinders were inserted into the test section just before the experiments by slightly emptying and then refilling the tunnel through the use of an auxiliary pump and a stainless-steel storage tank (50 gallons capacity). This procedure, employed in both tunnels and for all pre-mixing techniques, eliminated the possibility of the premature deposition of polymer on test bodies during the ageing period.

Subsequent investigations during the third and fourth years of the research indicated that an equally satisfactory and yet more expeditious mixing technique would be the direct feeding of the polymer powder into the tunnel. For this purpose, the powder was sprinkled, in a matter of minutes, in the amount desired, into the test section while the pump ran at its lowest speed. The tunnel provided the required agitation for the wetting action and the moving water (about 5 ft/s) allowed little chance of coagulation of the partially wetted particles. Then the solution was aged for approximately 24 h and the cylinder were mounted in the manner desired, as described above.

The addition of additives such as sucrose or polypropylene glycol, for the purpose of expediting the dissolving process, was considered but quickly discontinued since no special problems of mixing or coagulation were encountered with either of the two methods described above. From time to time and particularly in frequency repeat runs, solutions made from a single batch of polymer were used to check the possible effects of both the known batch-to-batch variation of the properties of a given polymer powder and of the degree of mixing provided by the two methods employed The results obtained through the use of the various procedures just cited did not show any measurable differences outside the usual experimental errors throughout the course of the investigation.

The tunnel and all the auxiliary components, including the pressure-gauge piping, were flushed three times prior to mixing a new solution. Water data were taken after chemically treating the tunnel with potassium bichromate, allowing 72 h to degrade any residual polymer, and then flushing three times with tap water. For the case when distilled water was used to prepare a 5 p.p.m. solution, the tunnel was flushed with 1500 gallons of distilled water prior to filling the tunnel and the storage tank.

Particle suspensions *in water* were prepared as follows. Spherical polystyrene beads (of specific gravity $1 \pm 0{\cdot}02$ and diameters 0·294 mm or 0·415 mm) and nylon fibres (of specific gravity $1{\cdot}14 \pm 0{\cdot}05$, diameters 0·028 mm and 0·020 mm, and length-to-diameter ratios 71·5 and 100) were sprinkled into the test section, in the amounts desired, and the main pump was allowed to run for approximately 5 h prior to inserting the test bodies and making direct drag measurements and pressure measurements.

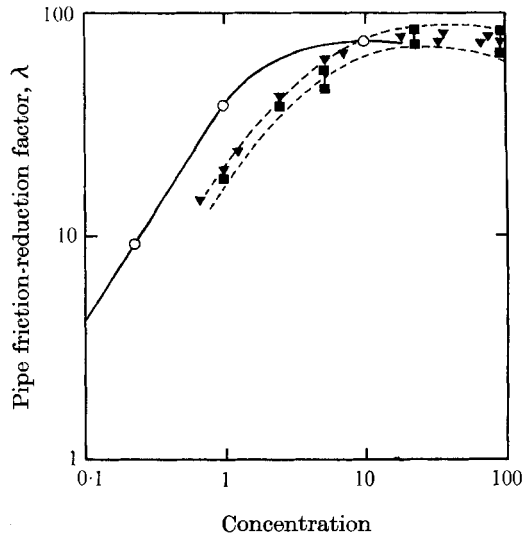

FIGURE 1. Pipe friction-reduction factor λ as a function of concentration. ○, laboratory-standard samples. Samples mixed in the tunnel: ■, by sprinkling polymer powder; ▼, through the use of master solutions prepared in a barrel.

2.5. *Percentage friction reduction*

The friction-reducing effectiveness of the polymer solution was determined with a turbulent-flow pipe rheometer, identical in principle to that pioneered by Hoyt (1965) and used by White & McEligot (1969). Tunnel samples of fresh solutions were tested as well as samples of solutions taken every 10 to 30 minutes of pumping, depending on the particular measurements made and the polymer concentration. Sufficient fluid was withdrawn from the tunnel to allow three flushes of the rheometer prior to two friction tests.

The percentage pipe friction-reduction parameter λ for each sample was calculated from

$$\lambda = 100(f_t - d)/(f_t - 64/Re),$$

where f is the friction factor for the sample solution and f_t is the Fanning friction factor for tap water, determined with the same rheometer for the Reynolds-number range of 3950–5660. It had a systematic error of approximately 3% below the expected smooth-pipe value. The error in repeatibility was of the order of 2%.

The percentage pipe drag-reduction factors λ for the solutions prepared in the tunnel, through the use of a master solution and by sprinkling dry powder, and aged 24 hours are compared in figure 1 with those obtained with master solutions prepared in a barrel. Apparently, in the range where λ is sensitive to concentration and in particular to *in situ* molecular weight, the solutions mixed in the tunnel are somewhat degraded relative to standard samples. The agreement between the λ values for the solutions prepared in the tunnel through both methods favours the explanation of relative degradation by pump action rather than the conjecture of incomplete dissolution of the polymer. Be that as it may,

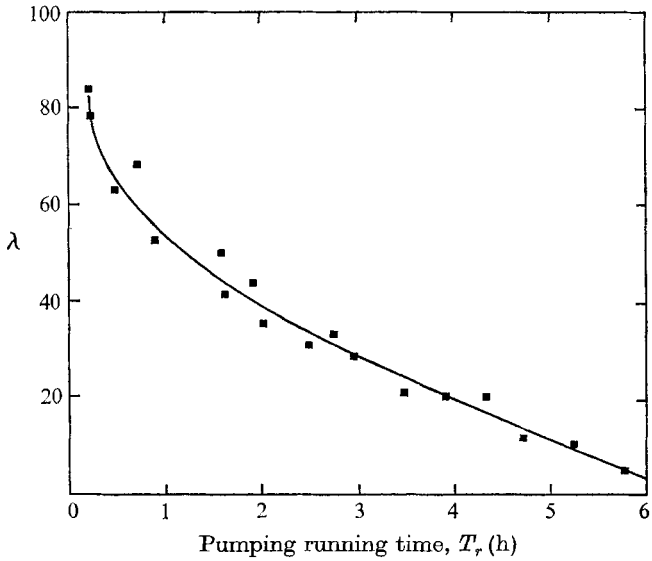

FIGURE 2. Sample data showing the decrease of the pipe friction-reduction factor due to shear degradation as a function of pump running time T_r for a 25 p.p.m. concentration and test-section velocity of $U = 12$ ft/s.

the results have shown that it is not the fairly fresh solution but rather sufficiently degraded solutions ($\lambda < 20$) that cause major changes in the drag-crisis region. Thus a comparative value of the percentage drag reduction was all that was needed and the mixing and friction-measurement techniques adapted here satisfactorily fulfilled this purpose.† Finally, degradation curves were obtained for concentrations of 5, 10, 25, 50 and 100 p.p.m. and for various cylinders mounted in the test section as a function of the total pump running time T_r. Only the one for 25 p.p.m. and a 1 in. cylinder is presented in figure 2 for the sake of brevity. Apparently, the rate of degradation slows down considerably once the components of the molecular weight distribution corresponding to high molecular weights have been preferentially attacked by the non-uniform turbulent shear field in the tunnel.

2.6. *Separation angle*

The separation of flow at several sections of the cylinder was observed by dye injection from the cylinder surface. The location of separation was measured by injecting dye aft of the separation point and then rotating the cylinder forward

† There does not appear to be a unique way of expressing the degree of shear degradation and its dependence on concentration, molecular distribution, etc. In view of this and other facts such as the failure of the intrinsic viscosity to correlate the drag reduction in pipes for fixed concentration and flow rate (Paterson & Abernathy 1970) and the inapplicability of the Merrill, Smith, Shin & Mickley (1966) and Merrill, Smith & Chung (1966) intrinsic-viscosity molecular-weight relation ($[\eta] = 1{\cdot}03 \times 10^{-4} M_w^{0.78}$ at 25 °C) to degraded solutions where the ratio of weight-average to viscosity-average molecular weight does not remain constant (Florey 1953), the simple method of friction-reduction measurement adopted here was preferred to other more complex methods in obtaining a repeatable measure of the degree of degradation.

while reducing the injection rate until 2° aft of the apparent separation point. The dye injection was then reduced to a minimum and the actual separation point was observed. The reported angle is the minimum angle at which separation occurred and is considered to be accurate to within $\pm 1°$ in those cases where separation was steady. In the case of unsteady separation (to be discussed in §3.2.2) caused by the flow of degraded solutions, the reported minimum separation angle is considered to be reliable to within $\pm 3°$.

2.7. *Corrections to drag and pressure coefficients*

The standard correction factors for wake and solid blockage have been uniformly applied *to all cylinder drag coefficients* through the use of formulae devised by Pope & Harper (1966). The pressure distributions are plotted in terms of corrected pressure coefficients C_p, unless otherwise noted, through the use of the relationship derived by Maskell (1965). The drag coefficients are plotted as a function of $Re\,(= Ud/\nu$, where ν is the kinematic viscosity of water at the measured fluid temperature). The standard practice has been to equate the viscosity of a dilute solution to that of water at the same temperature. This was the procedure followed during the present investigation.

2.8. *Anticipated experimental errors*

The measurements of the stagnation pressure and direct drag measurements were the most critical, since the correlation of the data was based on these measurements. Stagnation-pressure error was estimated to have introduced a relative error of 3 %. Drag-force measurements were assumed to have an error of 5 %. These errors resulted from calibrations, balance, the reading of the recorder chart paper, etc.

Strouhal frequency measurements had an approximately 2 % error based on the comparison between different methods of testing (for a comprehensive summary of these methods and the comparison of various results see Popov 1966; Lienhard 1966). Root–mean–square frequency measurements were averaged over certain time periods at various sample rates and compared with a Fourier frequency analysis of the same signal. This resulted in a ± 1 Hz error for a 30 Hz signal.

The wake-width measurements depended on the observer's ability to determine the initiation of velocity spikes. Thus no estimate of the error involved is possible.

3. Results

3.1. *Water flow*

Reference determinations of the direct-drag and pressure-integrated drag coefficients, separation angle, vortex-shedding frequency, frequency spectrum, and pressure distribution were made in pure-solvent flow for comparison with similar data obtained in the polymer-solution and suspension flows. The water data were also compared with existing drag and frequency data obtained primarily in air.

3.1.1. *Drag coefficients.* The direct-drag and pressure-drag coefficients (both

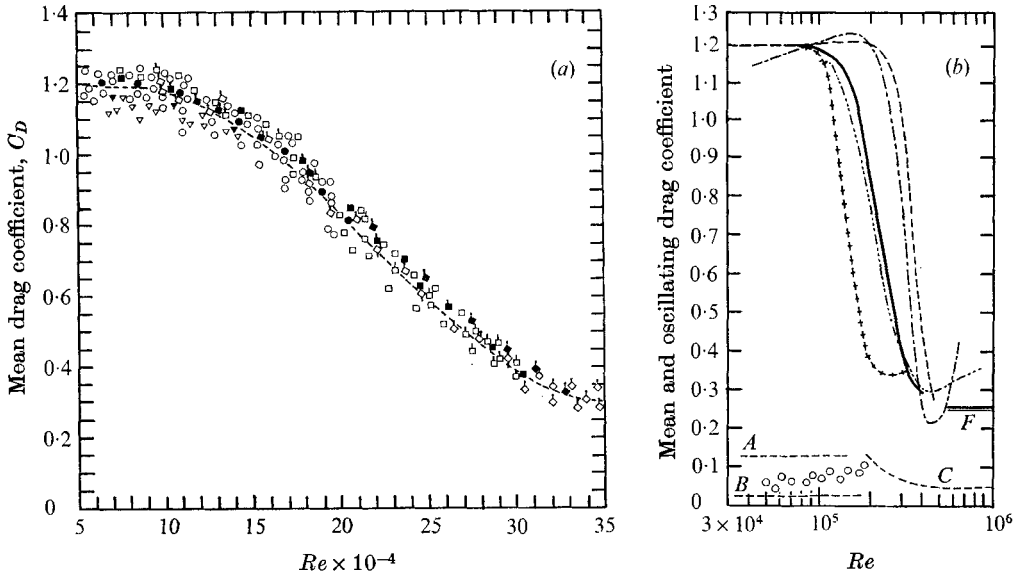

FIGURE 3(*a*). Mean-drag coefficient C_D *vs.* *Re* (pure-solvent flow). Solid symbols denote data obtained through pressure integration, open symbols represent those obtained through direct drag measurement and flagged symbols (solid or open) denote data obtained in the larger test section. Cylinder sizes: ▽, ▼, 0·75 in.; ○, ●, 1 in.; □, ■, 1·5 in.; ◇, ◆, 1·97 in. (*b*) Comparison of the mean-drag coefficient C_D for pure-solvent flow with other data: ——, present study; – –, Delany & Sorenson (1953); –·–, Humphreys (1960); –···–, Bublitz (1971); +, NPL data (Goldstein 1965); *F*, Fung (1960). Oscillating drag coefficient *vs.* *Re*: *A*, maximum values by Drescher (1956) and Humphreys (1960); *B*, maximum values by McGregor (1957); ⊙, present study; *C*, r.m.s. values by Fung (1960).

corrected for tunnel-wall constraint) are plotted in figure 3(*a*) against *Re* for four sizes of cylinders in the range of transitional Reynolds numbers. These data are compared in figure 3(*b*) with some of the existing data (all represented by faired lines) obtained primarily in air (Goldstein 1965, p. 156 (NPL data); Delany & Sorenson 1953 (NACA data); Humphreys 1960; Bublitz 1971). Apparently, the present data lie between the results obtained at NPL and NACA. The differences between the various curves are primarily attributable to the difference in the turbulence levels of various tunnels (Fage & Warsap 1973; see also Schlichting 1968, p. 622; Lienhard 1966). According to the experiments of Fage & Warsap (1930), the transitions are shifted strongly to the lower Reynolds numbers with increasing disturbance. A variation in upstream turbulence does not appear to alter the severity of the 'dip' in C_D (Mair & Maull 1971). However, the effects of surface roughness and tripping wires alter transition characteristics. In other words, the earlier the transition begins, the higher the value of the drag coefficient in the supercritical range and the sharper the rate of drop in the transition curve. Apparently, roughness modifies the existent boundary layer to such an extent that the instability of the modified flow is encountered (Fage & Warsap 1930; Achenbach 1971).

Also shown in figure 3(*b*) are the maximum values of the amplitudes of oscillation (often at twice the eddy-shedding frequency, sometimes randomly about a

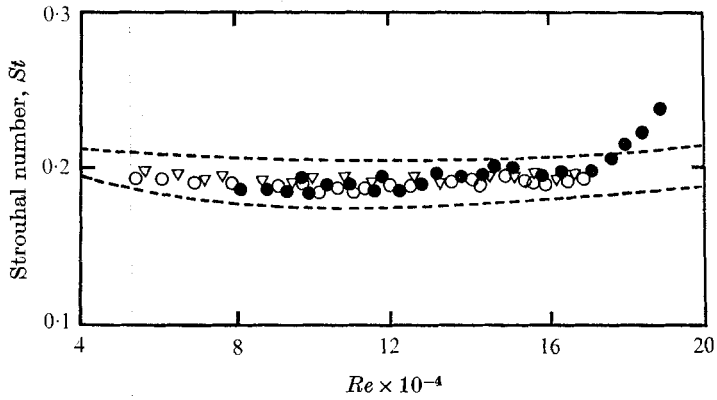

FIGURE 4. Strouhal *vs.* Reynolds number for pure-solvent flow. – – – –, limits of data compiled by Lienhard (1966); ▽, 1 in. perspex cylinder; ○, 1 in. aluminium cylinder; ●, 1·5 in. perspex cylinder.

mean value) in C_D together with the corresponding maximum limiting values (represented by faired lines) obtained by Drescher (1956); McGregor (1957) and Humphreys (1960), and the corresponding r.m.s. values obtained by Fung (1960) in the higher range of Re. The best that one can infer from these measurements of the oscillating drag force is that the drag in air or pure water is relatively steady and that its maximum deviation (about 15%) occurs in the boundary-layer transition regime.

In the absence of roughness and excessive free-stream turbulence, the transition in drag coefficient between $Re \approx 10^5$ and $Re \approx 7 \times 10^5$ is currently interpreted (e.g. Roshko 1961; Tani 1964; Batchelor 1967, p. 342; Jones, Cincotta & Walker 1969) to be due to transition of the separated boundary layer to a turbulent state, the formation of a separation 'bubble', reattachment of the rapidly spreading, turbulent, free shear layer, and finally, separation of the turbulent boundary layer at a position further downstream from the first point of laminar separation. The reduction of the wake size as a consequence of the retreat of the separation points then results in a smaller form drag. The subsequent increase in C_D between $Re \approx 10^6$ and $Re \approx 10^7$ is then interpreted to be a consequence of the transition to a turbulent state of the attached portion of the boundary layer.

3.1.2. *Vortex-shedding frequency.* A plot of the Strouhal number St versus Re is presented in figure 4 for two sizes of cylinders and two types of mounting conditions. Also shown in this figure is the envelope of the previous data collected and compiled by Lienhard (1966). This region is shown without data points since the individual points are prohibitively packed and overlapped. The present data lie amongst the existing data, obtained mostly with a hot-wire anemometer in air. Furthermore, as will be noted subsequently, they are fully substantiated by both the frequency spectrum measurements of the pressure fluctuations on the cylinder and of the velocity fluctuations in the wake of the cylinder.

3.1.3. *Frequency spectrum of the wall-pressure fluctuations.* Figure 5 represents typical plots of r.m.s. filter output versus frequency for various Re. A typical Fourier analysis for $Re = 10{\cdot}7 \times 10^4$ is shown in figure 6. Both plots show, for

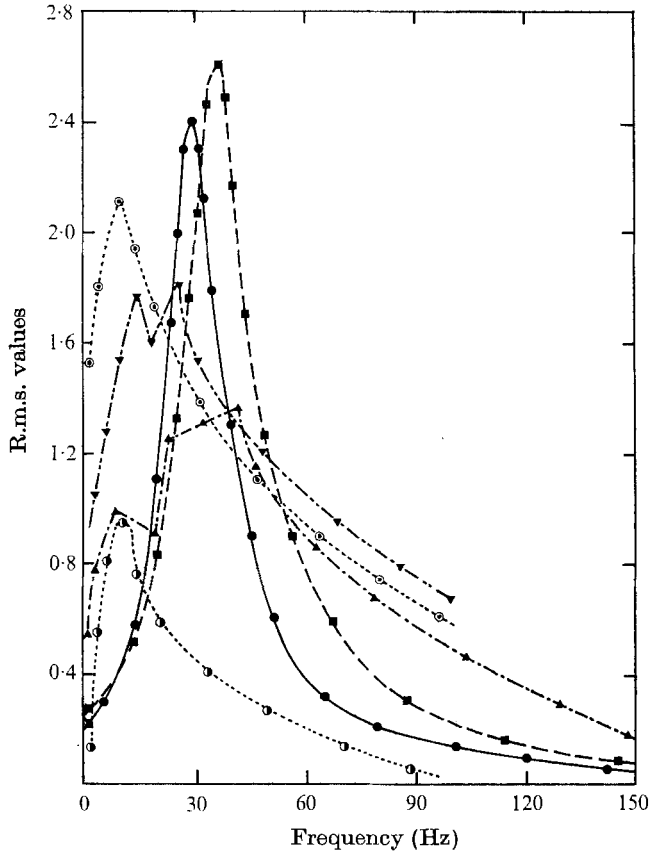

FIGURE 5. A typical r.m.s. *vs.* frequency plot for cylinders in pure-solvent flow. Values of $Re \times 10^{-4}$: ◑, 7·9; ●, 9·6; ■,12; ▲, 16; ⊙, 24·6; ▼, 15.

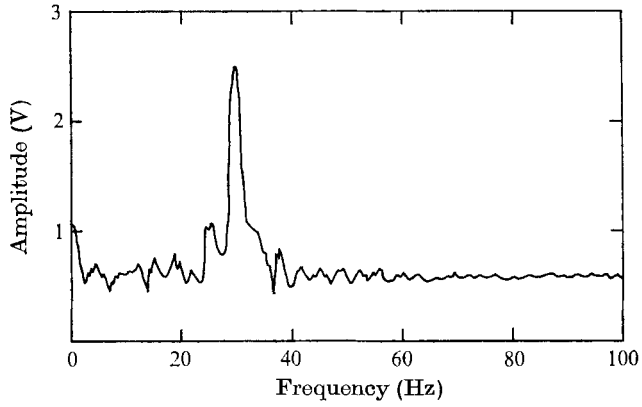

FIGURE 6. A typical Fourier analysis for $Re = 10{\cdot}7 \times 10^4$ (solvent flow).

$Re = 10{\cdot}7 \times 10^4$, a maximum amplitude at 30 Hz which corresponds to the expected and previously recorded Strouhal frequency. The frequencies of the maximum r.m.s. amplitudes for all the other Re, except $Re = 24{\cdot}6 \times 10^4$, again corresponded to the previously measured St values. For $Re = 24{\cdot}6 \times 10^4$ the flow

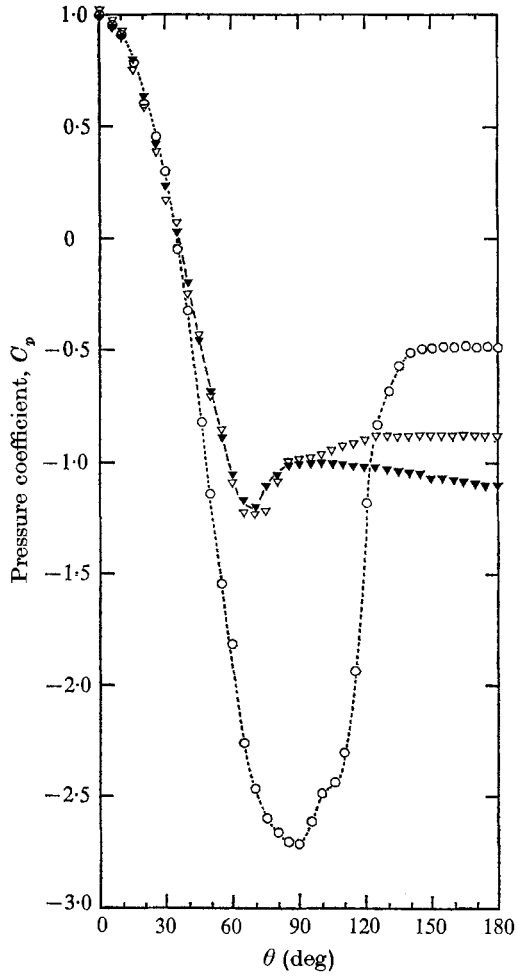

FIGURE 7. Representative pressure distributions in solvent flow: ▼, $Re = 10{\cdot}7 \times 10^4$; ▽, $Re = 16{\cdot}2 \times 10^4$; ○, $Re = 24{\cdot}8 \times 10^4$. [For the corresponding C_D values, see figure 3(*a*).]

is well into the transition region and has lost all the predominant frequencies except for a very low frequency wave modulated with high frequencies. The loss of the regular vortex shedding in the transition region is attributed by Bearman (1969) to the gross three-dimensionality of the flow caused by turbulent wedges immediately in front of the cylinder. This explanation acquires a new significance in view of the fact that the regular vortex shedding in polymer solutions ceases, as will be seen later, at relatively smaller Reynolds numbers.

3.1.4. *Pressure distributions.* The pressure coefficient C_p curves (corrected for tunnel-wall constraint) are plotted in figure 7 against the angular position θ for three representative Reynolds numbers. It is seen that a separation bubble is present only at the highest Re as shown by the inflexion point (see e.g. Roshko 1961; Tani 1964; Jones *et al.* 1969) in the C_p curve near $\theta \simeq 110°$. The variation of the position of the separation point with Re will be discussed later (for ease of comparison) together with that corresponding to the polymer-solution flow.

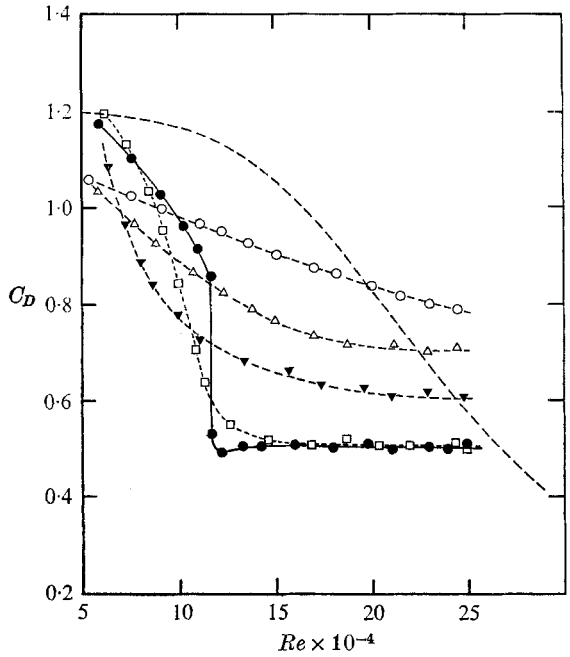

FIGURE 8. Variation of the drag coefficient with Re and λ for a 1 in. cylinder in the flow of a 25 p.p.m. concentration polymer solution – –, solvent data from figure 3(*a*); ○, $\lambda = 82$; △, $\lambda = 45$; ▼, $\lambda = 30$; □, $\lambda = 13$; ●, $\lambda = 9$.

3.2. *Polymer-solution flow*

3.2.1. *Drag coefficients.* Figure 8 shows the variation of the drag coefficient for the flow of both fresh and degraded 25 p.p.m. solution about a 1 in. cylinder. Also included in this figure is part of the best-fit curve to the water drag shown in figure 3(*a*). It is immediately apparent that the additive and in particular its degradation (*in situ* lower molecular weight) with time cause remarkable changes in the transition region. In fresh solutions (with relatively high values of λ), the variation of C_D with Re is similar to that found in sphere-drop tests (e.g. A. White 1967) and cylinder tow-tank tests (e.g. McClanahan & Ridgely 1968). In other words, fresh or fairly fresh solutions yielded drag coefficients which monotonically decreased from approximately 1·1 down to 0·6 or so as Re increased from about 5×10^4 to about 3×10^5 (the upper range of Re depending on the size of the particular cylinder used) for all the cylinders tested. When the degradation reached a sufficiently high state, i.e. when λ reached a sufficiently low critical value λ_c, a new and entirely unexpected flow behaviour was established which had as dramatic an effect on the drag coefficient as a tripping wire or roughness element. Indeed, a critically degraded solution yielded a fairly steady, low drag coefficient ($C_D \simeq 0{\cdot}5$) above a critical value of Re, a C_D of about 0·9 just below the critical Re, and a dual value in drag force and hence in C_D at $Re = Re_c$. The occurrence of the drag crisis was accompanied by unsteady flow patterns (as observed with dye injection) near the separation line. These observations are discussed in detail in §3.2.2. At a velocity slightly larger (approximately 0·3 ft/s) than that

Cylinder size, d (in.)	Concentration (p.p.m.)	Minimum $Re_c \times 10^{-4}$	Minimum C_D above Re_c	Time to critical state T_r (min)	Critical λ_c (maximum)
0·50†	5	11·1	0·42	82	10–8
0·50	5	11·5	0·42	85	11
0·75	5	11·2	0·45	78	12
1·00	100	10	0·56	820	7·5
1·00	25	11·4	0·51	300	9
1·00	5	10·5	0·41	72	10
1·00‡	5	10	0·40	130	11
1·00	2·5	10·5	0·46	35	12
1·00	1	11	0·47	10	10·2
1·50	100	11·8	0·58	780	11
1·50†	25	10·7	0·59	275	11·3
1·05†§	25	11·5	0·55	220	10·5–9
1·50	5	10·2	0·44	120	12
1·50§	5	11	0·47	95	11·5
1·97†§	10	10·7	0·45	155	12·5–10
1·97§	5	11·8	0·42	90	12
1·97§	2·5	10·5	0·40	25	11

† From wall-pressure measurements. ‡ Solvent: distilled water.
§ In the larger test section.

TABLE 1. Measured values at the first initiation of the drag crisis

corresponding to Re_c, oscillations in drag decreased sharply and drag remained quite steady at the lower supercritical value.

Table 1 summarizes the type of information contained in figure 8 for all other cylinders and concentrations tested. It is noted, in passing, that the only significant consequence of the use of distilled water as the solvent is to reduce the rate of degradation or increase the time T_r necessary to reach a given λ. At nearly equal values of λ, however, both the filtered solution of polymer in tap water and that of polymer in distilled water produced drag coefficients and drag crisis at velocities which differed by less than the expected experimental error.

The effect on C_D of the additional degradation of a given solution beyond the first occurrence of the drag crisis was studied by running the pump until the solution produced essentially no friction reduction in the rheometer, i.e. as $\lambda \to 0$. As a representative example, figure 9 shows that Re_c gradually increases (eventually approaching the value for the solvent), and C_D increases towards the solvent values for $Re < Re_c$ and remains approximately constant for $Re > Re_c$.

The relative importance of concentration on the occurrence of the critical state is revealed by figure 10. Evidently, C_D was affected primarily in the region where $Re > Re_c$, larger concentrations producing relatively larger C_D values. As for the minimum value of Re_c (corresponding to the first occurrence of the drag crisis), it varied only from $9{\cdot}5 \times 10^4$ to about 12×10^4, whereas the concentration varied by a factor of 100, T_r by a factor of 80, and the cylinder diameter by a factor of 4 as is shown by the representative data shown in figure 10 (see also table 1). Thus, concentration, within the range of values tested, has little or no effect on the occurrence of the critical state.

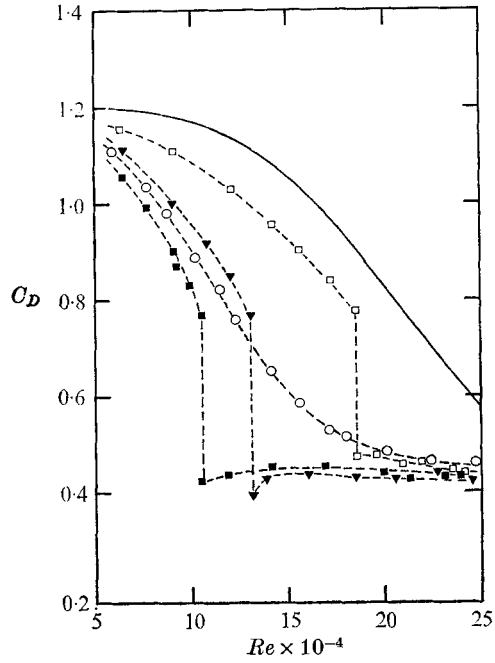

FIGURE 9. Evolution of C_D and Re_c with increasing degradation for a 1 in. cylinder in the flow of a 2·5 p.p.m. concentration polymer solution: – –, solvent data from figure 3(*a*); ○, $\lambda = 40$; ■, $\lambda = 12$; ▼, $\lambda = 8$; □, $\lambda = 2$.

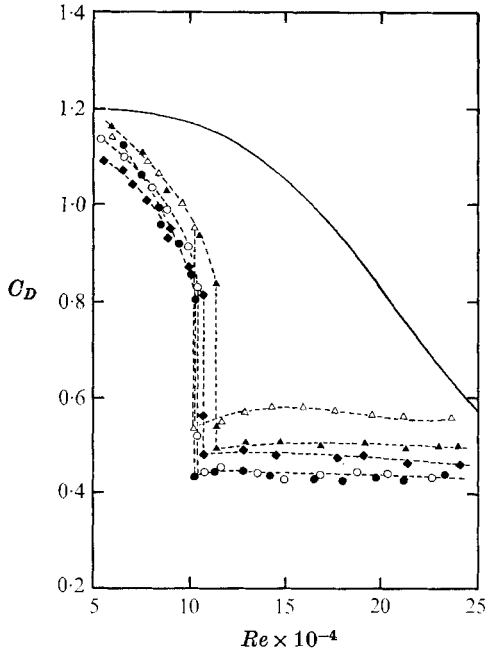

FIGURE 10. The first occurrence of the drag crisis for a 1 in. cylinder in the flow of polymer solutions. Concentrations: △, 100 p.p.m.; ▲, 25 p.p.m.; ○, 5 p.p.m. (distilled water); ●, 5 p.p.m.; ◆, 1 p.p.m. (See table 1 for the corresponding λ_c values.)

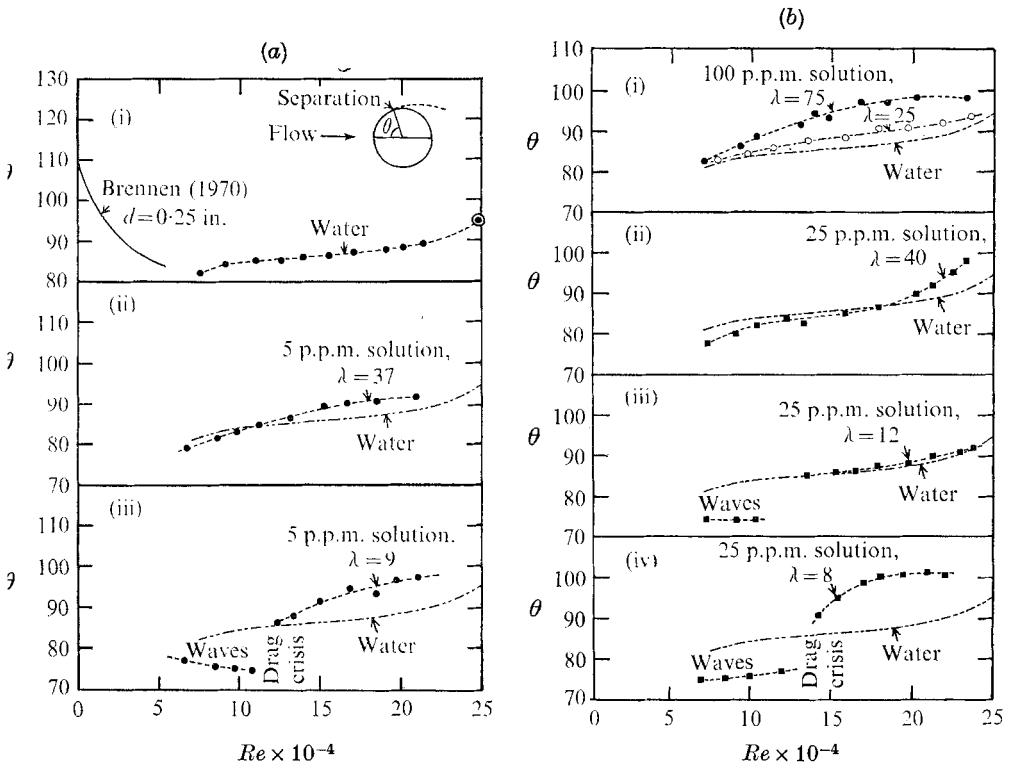

FIGURE 11. Angle of separation θ *vs. Re.* (*a*): (i) Water: ●, 1 in., ⊙, 1·5 in. (ii) 5 p.p.m. polymer solution with λ = 37. (iii) 5 p.p.m. solution with λ = 9. (*b*) 100 p.p.m. and 25 p.p.m. solutions for various values of λ.

3.2.2. *Separation angle and the observations of the separated flow.* Representative values of the separation angle for both the solvent and polymer-solution flow are presented in figures 11 (*a*) and (*b*). All the separation-angle data have shown that fresh solutions ($\lambda \gg \lambda_c$) yield relatively larger separation angles in the range of Reynolds numbers tested and that the effect of degradation is to move the separation line gradually closer to that for the pure solvent. For such solutions for which there was no drag crisis but rather a gradual decrease in the drag coefficient (see figure 8), the dye filament injected far upstream of the separation line gradually blurred, signifying a large-scale instability and/or gradual transition from a laminar to a turbulent boundary layer prior to separation and the absence of a laminar separation bubble. These observations cannot, for obvious reasons, be substantiated by hot-film measurements. The existence of the large-scale instability can be inferred only from pressure measurements and direct observations by camera or eye of the motion of dye filaments. The difficulties of observation, measurement and proper interpretation even in simpler cases of boundary-layer transition have been recently described in masterly fashion by Klebanoff & Tidstrom (1972).

A similar type of turbulent transition and a shift of the separation line to a point between normal laminar and turbulent separation in fresh solutions of

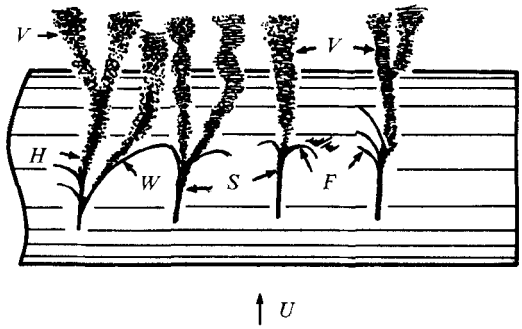

FIGURE 12. Separated flow patterns at $Re = Re_c$. V, streamwise vortex lines; H, dye enters the free-shear layer; W, dye remains close to the cylinder wall; S, unsteady separation point; F, fine dye streaks.

Polyox WSR-301, at comparable concentrations, was also noted by Lang & Patrick (1967) in their sphere-drop tests in a tank of otherwise quiescent water. They have also noted that the shift in turbulent separation point increased with increasing concentration of the additive.

As λ and Re approached their respective critical values over a narrow range (Re 8×10^4 to 10^5 and λ from about 14 to 10, for the first critical state; see also figures 8–10), air as well as dye injected upstream of the apparent separation point revealed distortions in the separation line and wavy separation patterns (spanning over cylinder angles of 5–10°) with subsequent transition to a turbulent boundary layer.

At $Re \simeq Re_c$ and $\lambda \simeq \lambda_c$ (spanning a very narrow range of Re from 10^5 to $1{\cdot}18 \times 10^5$ for all the concentrations tested), observations by injecting dye at a minimum injection velocity revealed an even more interesting unsteady flow pattern (see figure 12). The position of the distorted separation line oscillated back and forth; the separated dye filament fluctuated with low and high amplitude both in the plane normal to the main flow and in the plane parallel to the main flow; dye streaks which remained close to the cylinder surface actually curved from their plane and became almost perpendicular to the ambient flow at an angle of approximately 100°; streams of dye, the tips of which did not remain close to the cylinder, acquired a longitudinal vorticity component in the direction of the main flow (resembling streamwise vortex filaments with a spiral type of unsteady vortex breakdown ; see e.g. Sarpkaya 1971); and in addition, to further complicate the picture, fine lines of dye formed approximately normal to the main dye stream.

At a slightly (approximately 0·3 ft/s) higher velocity than that corresponding to the particular Re_c in a given test run, the separation line (no longer a wave) switched downstream and remained steady. However, the most significant observation in this range is that the dye became blurred a few degrees upstream of the separation line, indicating once again a transition from laminar to a turbulent flow in the boundary layer at or just prior to separation as in the case of fairly fresh solutions, as previously noted.

The fact that the foregoing description of the motion of separated flow occurs on cylinders rigidly spanning the test section rules out the possibility that the

observed unsteady flow patterns at $Re = Re_c$ and $\lambda = \lambda_c$ are a spurious phenomenon resulting from the vibration of the test cylinder and its support. It rather appears that the polymer can cause significant instabilities in the boundary layer around the cylinders and that the form, the intensity, the subsequent convection and evolution, and the interaction with the boundary layer of these instabilities depend on the prevailing values of Re and λ in non-cavitating flows, resulting in a wide variety of transition and separation phenomena.

The only other observation of the wavy separation lines and the flow patterns sketched in figure 12 is that by Brennen (1970). He found such instabilities to be independent of concentration and weakly dependent on degradation. Our observations have shown such instabilities to be critically dependent on Re and λ. Thus an attempt to explain or reconcile the differences between the two observations is called for. First and most important, Brennen's experiments deal with flows with ventilated cavities whereas the present work relates only to non-cavitating flows. The cavity separation point in Brennen's experiments is determined, as he pointed out, by the smooth separation condition as a function of the prevailing cavitation number. In the present case, in the range of Reynolds numbers corresponding to those of Brennen (for a cylinder, his maximum Re was about 5×10^4, i.e. *the lower range of our Re*), the flow is far from the critical state and neither the separation point nor the drag coefficient is affected by the presence of polymer regardless of its concentration (1–200 p.p.m.) The fact that this is so has also been verified by others (e.g. Lang & Patrick 1967; A. White 1966, 1967). Thus, the facts recorded by Brennen regarding the relationship between the occurrence of the instabilities and concentration in a flow with ventilated cavities at subcritical Reynolds numbers cannot simply be contrasted with those for the instabilities observed in a non-cavitating flow at or near critical Reynolds numbers. The only conclusion that can be drawn from the observations is that instabilities also occur in comparable fully attached flows (as anticipated by Brennen), but at higher Reynolds numbers where the stability and separation conditions radically depart from those of smooth separation.

3.2.3. *Drag- and pressure-frequency spectrum measurements and Strouhal frequency.* The r.m.s. data, similar to those plotted against frequency in figure 13, have shown that the amplitude of the r.m.s. signal for the polymer solution decreases with increasing degradation up to a certain value of λ. With further degradation, a state is reached ($\lambda \simeq 20$) where the minimum frequency spectrum is almost flat. The return to solvent-like behaviour is accomplished by degrading the polymer further. It is rather remarkable that, for the data shown in figure 13, the polymer solutions with $\lambda \simeq 7$ and $\lambda \simeq 86$ yield nearly the same r.m.s. values. This particular phenomenon, as well as the variation of the mean and fluctuating component of C_D, has been studied in great detail for specific frequencies (Kell 1971). The results may be best illustrated by plotting the maximum r.m.s. values for pressure and the mean-drag coefficient as a function of λ, as shown in figure 14 for a Reynolds number slightly less than critical and in figure 15 for a Reynolds number slightly larger than critical. It is apparent from figure 13 that when the r.m.s. value is relatively high or close to the solvent value say (1·4), a predominant Strouhal frequency is present (e.g. for $\lambda \simeq 86$ or $\lambda \simeq 10$, the dominant frequency

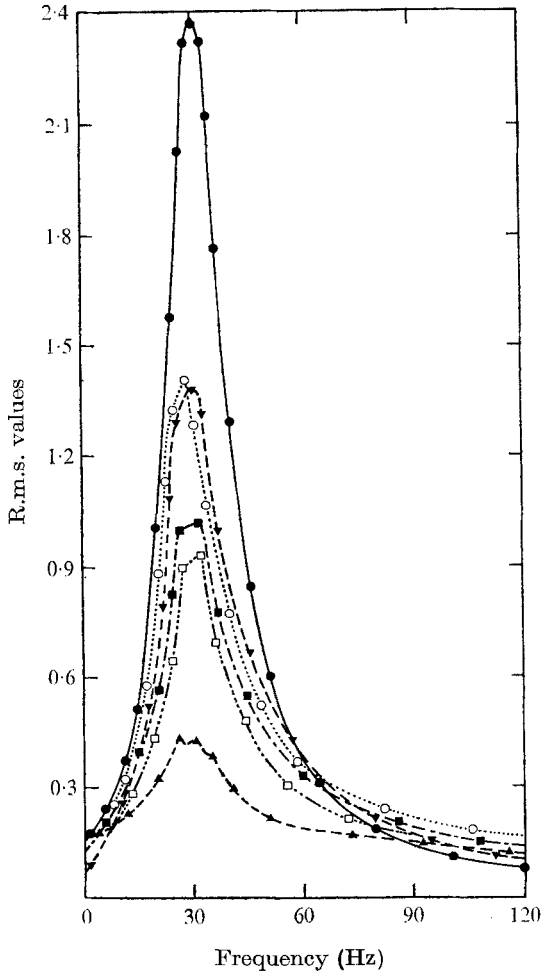

FIGURE 13. R.m.s. values for pressure fluctuations at $\theta = 120°$ plotted against frequency for a 1 in. cylinder in a flow of 25 p.p.m. solution at $Re = 10^5$. ●, $\lambda = 0$ (solvent); ▼, $\lambda = 86$; ■, $\lambda = 48$; ▲, $\lambda = 22$; □, $\lambda = 10$; ○, $\lambda = 7$.

is 30 Hz); when it is at a minimum (for $14 < \lambda < 20$), there is no dominant frequency. The drag crisis at a specific value of $\lambda < \lambda_c$ occurs (see figures 15 and 9) either with the rapid disappearance or the re-establishment of a dominant frequency depending on whether $Re \to Re_c$ from below or above.

3.2.4. *Pressure distribution.* Measurements have revealed that the pressure distribution about a cylinder in polymer-solution flow lies between the laminar and turbulent distributions for water for the range $0 < \theta < 100°$ and that the pressures over the rear half of the cylinder differ considerably depending on λ and concentration. The following points out these differences through the use of typical plots.

The pressure distributions around a 1 in. cylinder in the flow of a relatively fresh 100 p.p.m. solution at $Re = 7{\cdot}2 \times 10^4$ and at $Re = 2{\cdot}1 \times 10^5$ are shown in figure 16 together with that obtained in tap water at $Re = 2{\cdot}5 \times 10^5$. Also shown

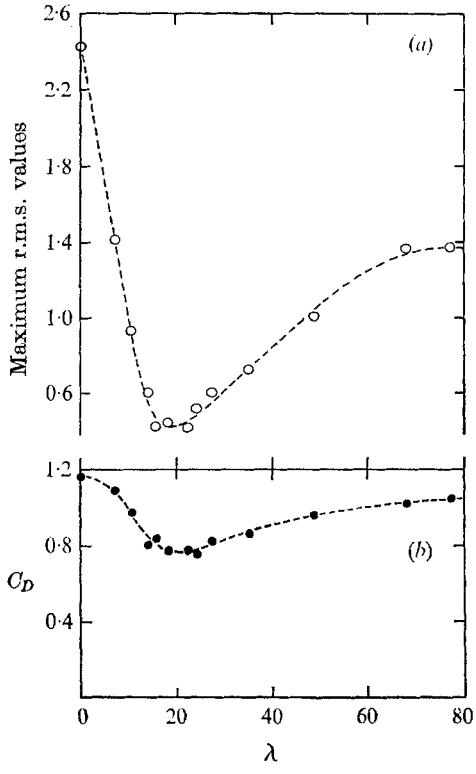

FIGURE 14. (*a*) Maximum r.m.s. values for pressure oscillations at $\theta = 120°$ *vs.* λ and (*b*) C_D *vs.* λ for a 1 in. cylinder in a flow of 25 p.p.m. solution, both at $Re = 10^5$ ($Re < Re_c$).

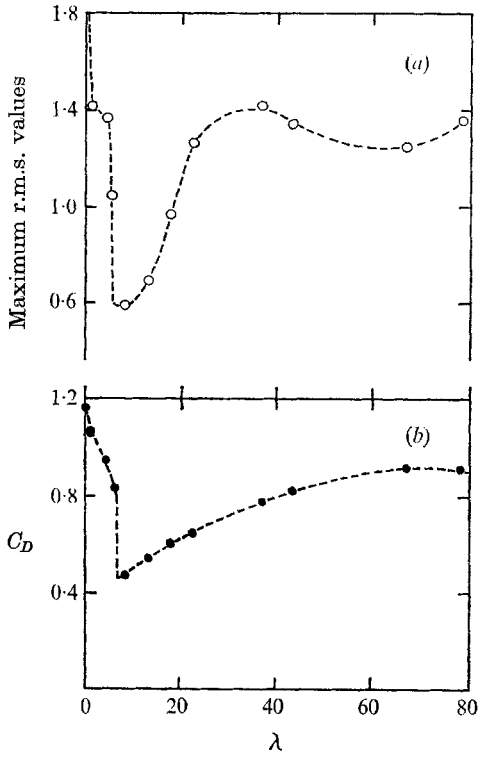

FIGURE 15. (*a*) Maximum r.m.s. values for pressure oscillations at $\theta = 120°$ *vs.* λ and (*b*) C_D *vs.* λ for a 1 in. cylinder in a flow of 25 p.p.m. at $Re = 12 \times 10^4$ ($Re > Re_c$).

in figure 16 is the pressure distribution obtained by Jones *et al.* (1969) in the Langley transonic tunnel around a 3 ft diameter cylinder at $Re = 8{\cdot}27 \times 10^6$ ($M = 0{\cdot}177$ and $C_D = 0{\cdot}583$). The pressure distribution at $Re = 7{\cdot}2 \times 10^4$ is typical of that found in the subcritical range in solvent flow. The one at $Re = 2{\cdot}1 \times 10^5$ is typical of that corresponding to the lower drag region in *all fresh solutions.*

As the Reynolds number increased from $7{\cdot}2 \times 10^4$ to $2{\cdot}1 \times 10^5$, the magnitude of the base pressure decreased, the magnitude of the minimum C_p increased and its location on the cylinder moved downstream from 70° to 80°. Evidently, the pressure distribution obtained with tap water at $Re = 2{\cdot}5 \times 10^5$ is markedly different from that obtained with the 100 p.p.m. solution at the corresponding values of Re and C_D. Equally evident is the strong similarity between the pressure distribution obtained by Jones *et al.* (1969) in the transcritical region and that obtained with the polymer-solution flow in the low drag region. The apparent implication of this similarity is that the more disturbed the flow by the presence of the polymer the lower the Reynolds number at which turbulent flow sets in before laminar separation occurs.

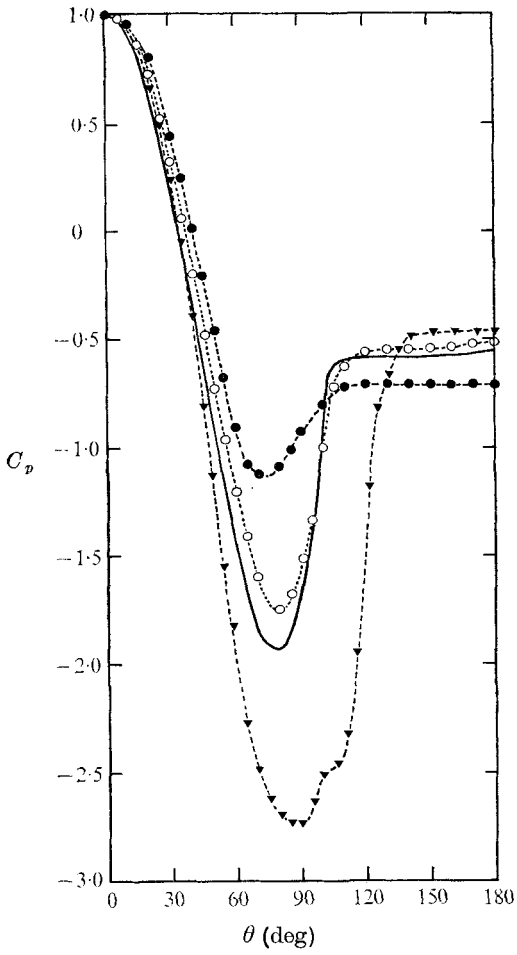

FIGURE 16. Characteristic pressure distributions in water, air and polymer-solution flows. ▼, $Re = 24{\cdot}8 \times 10^4$, $C_D = 0{\cdot}6$ (water); ——, Jones *et al.* (1969), $Re = 8{\cdot}27 \times 10^6$, $M = 0{\cdot}177$, $C_D = 0{\cdot}583$ (air); ●, $Re = 7{\cdot}2 \times 10^4$, $C_D = 0{\cdot}96$ (100 p.p.m. solution with $\lambda = 75$); ○, $Re = 2{\cdot}1 \times 10^5$, $C_D = 0{\cdot}6$, (100 p.p.m. solution with $\lambda = 70$).

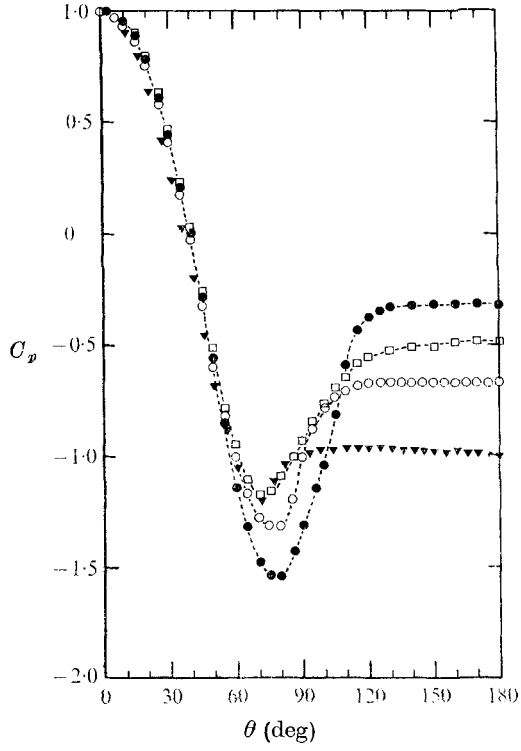

FIGURE 17. Evolution of the pressure distribution with degradation about a 1 in. cylinder in a flow of 25 p.p.m. solution at $Re = 13 \times 10^4$ ($> Re_c$): ○, $\lambda = 81$, $C_D = 0{\cdot}83$; □, $\lambda = 25$, $C_D = 0{\cdot}73$; ●, $\lambda = 9{\cdot}6$, $C_D = 0{\cdot}49$ (just prior to the occurrence of the drag crisis); ▼, water at $Re = 13 \times 10^4$.

The change in the pressure distribution with degradation was studied at $Re = 13 \times 10^4$ ($> Re_c$) with a 1 in. cylinder in a 25 p.p.m. solution. As shown in figure 17 (see also figures 8 and 9), the base-pressure coefficient changed from $-0{\cdot}67$ to $-0{\cdot}30$, the minimum C_p on the cylinder varied from $-1{\cdot}18$ to $-1{\cdot}56$ and C_D varied from 0·83 to 0·49 just before the occurrence of the drag crisis. It is immediately apparent from a comparison of the pressure data for water at the same Re (also shown in figure 17) with those for polymer solution that whereas the pressure on the front half of the cylinder is almost unaffected by the presence of polymer, the pressure on the rear half of the cylinder is significantly increased.

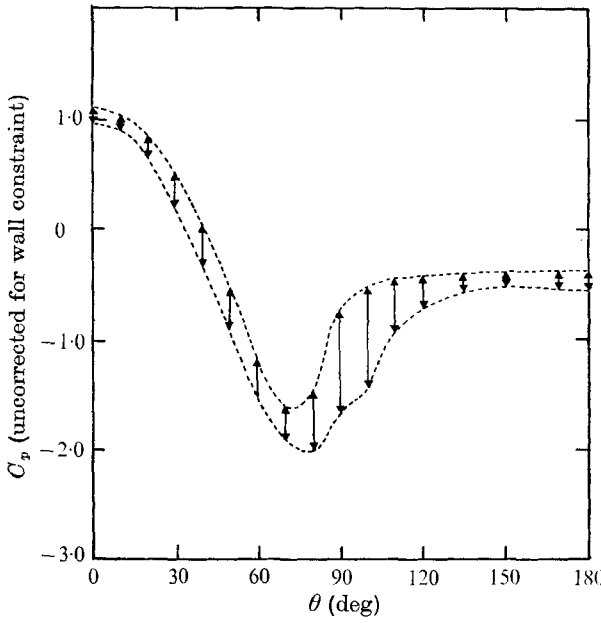

FIGURE 18. Large pressure oscillations (uncorrected for tunnel constraint) on a 1 in. cylinder for a critical state eventually occurring at $Re = 13 \times 10^4$ in a flow of p.p.m. solution with $\lambda = 7{\cdot}5$.

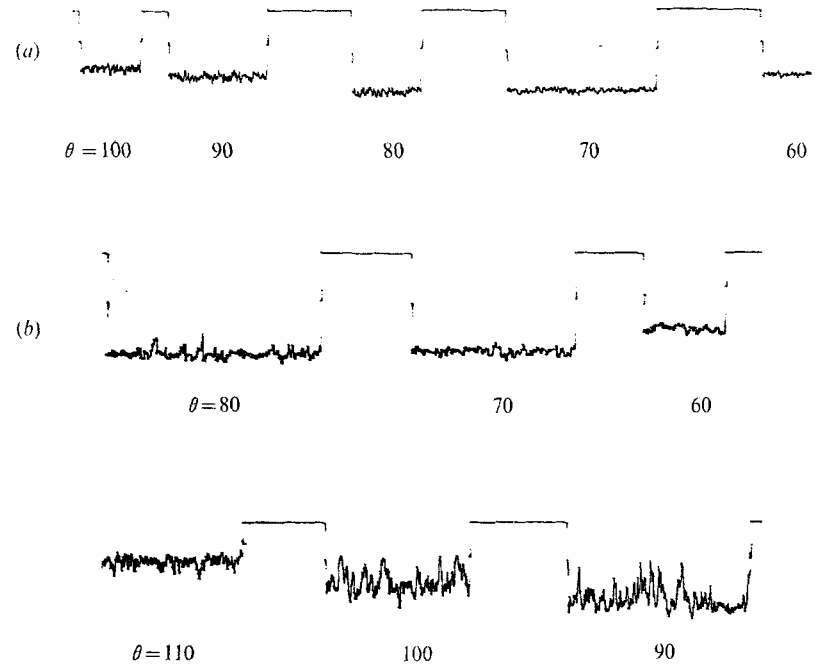

FIGURE 19. Sample pressure oscillations at various angles before and during drag crisis at $Re = 13 \times 10^4$ with a flow of 25 p.p.m. solution about a 1 in. cylinder. (*a*) For $\lambda = 20$ ($> \lambda_c$ at $Re = 13 \times 10^4$). (*b*) For $\lambda = 7{\cdot}5$ ($= \lambda_c$ at $Re = 13 \times 10^4$). All of the above recordings were made at 1 mm/s chart speed and at the same amplifier settings, i.e. identical attenuations and sensitivity settings.

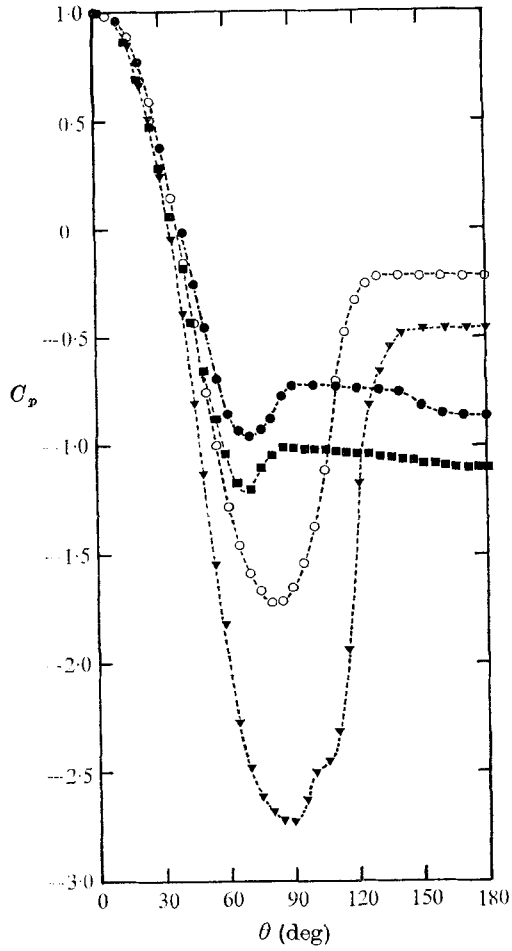

FIGURE 20. Typical pressure distributions on a 1 in. cylinder. With a flow of 5 p.p.m. solution before and after the onset of drag crisis: ●, $Re = 9{\cdot}6 \times 10^4$ ($< Re_c$); ○, $Re = 2 \times 10^5$ ($> Re_c$). With solvent flow: ■, $Re = 9{\cdot}6 \times 10^4$; ▼, $Re = 24{\cdot}8 \times 10^4$.

This observation, coupled with the fact that the separation angle, measured at time intervals between data sets, increased only from 82° to 86°, leads one to suggest that the characteristics of the near wake and the vortices comprising it are measurably affected by the polymer. This point will be discussed further in §3.2.5.

With increased pumping or degradation, the critical Re approached $1{\cdot}3 \times 10^5$. The resulting pressure distribution (uncorrected for tunnel-wall constraint) is plotted in figure 18. It indicates large pressure oscillations in the region of unsteady separation and smaller oscillations in the front and rear parts of the cylinder. Oscillograph tracings indicated the relatively low frequency (and large amplitude) of these oscillations as compared with the Strouhal frequency in tap water at the same Re. Sample pressure oscillation traces are shown in figure 19.

After a solution has degraded sufficiently to produce a dual value drag-coefficient region, two distinct pressure distributions developed, one at $Re > Re_c$

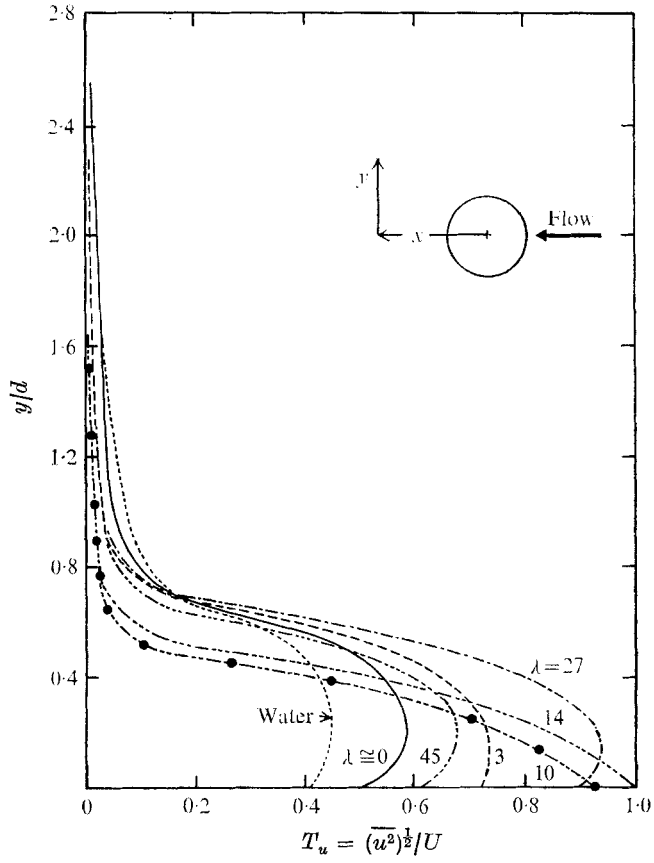

FIGURE 21. Typical turbulence-intensity profiles at $x = d$ and $Re = 12 \times 10^4$ for a 25 p.p.m. solution at various levels of degradation. Data points are shown only for $\lambda = 10$ for sake of clarity.

and the other for $Re < Re_c$. These two types of pressure distributions, on a 1 in. cylinder in a flow of 5 p.p.m. polymer solution, are shown in figure 20 together with those for water at the corresponding Reynolds numbers. The emerging fact is that the base pressure is considerably increased by the polymer both for $Re > Re_c$ and $Re < Re_c$, leading to the observed reduction in drag in the range $5 \times 10^4 < Re < 3 \times 10^5$.

The pressure distributions presented above are typical of those measured on 0·5 in., 0·75 in., 1 in., 1·5 in. and 1·97 in. cylinders at comparable velocities, concentrations and degradations during the entire investigation.

3.2.5. *Hot-film surveys of the near-wake flow field.* Exploratory measurements of turbulence and several other parameters were made inside and outside the wake of a 1 in. perspex cylinder in both tap-water and polymer solution (25 p.p.m.) flow for Reynolds numbers ranging from 8×10^4 to 14×10^4 and for representative values of λ. Traverses of the flow field along the y axis were made at $x = d$, $x = 1{\cdot}5d$ and $x = -3{\cdot}5d$, x representing the positive direction along the flow with the origin at the mid-point of the cylinder axis and y the other co-ordinate

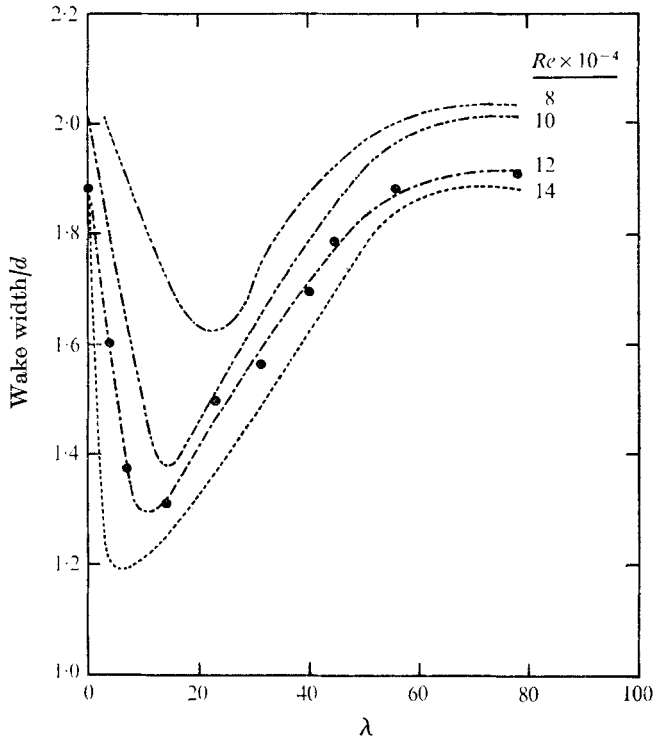

FIGURE 22. Wake width in terms of the cylinder diameter at $x = 1{\cdot}5d$ *vs.* λ for various values of Re for a 25 p.p.m. solution. Data points are shown only for $Re = 12 \times 10^4$ for sake of clarity.

in the x, y plane, which is the centre-plane of the cylinder. Reference measurements of the longitudinal component of turbulence, wake width, frequency spectrum and microscale of turbulence were made in tap water for comparison with similar data obtained in 25 p.p.m. polymer solution. Only the most representative results will be presented here since the complete details of the experiments are described in the thesis by Schimmels (1971).

The longitudinal component of the turbulence intensity T_u along the y axis at $x = d$ for a representative value of $Re = 12 \times 10^4$ is shown in figure 21 for various values of λ (data points are shown only for $\lambda = 10$ for sake of clarity). It is apparent from figure 21, as well as from other data not presented here, that T_u is *reduced* outside the wake, the maximum reduction occurring at $\lambda = 10$. In the region from $y = 0{\cdot}5d$ to $y = 1{\cdot}25d$, T_u diminished to 33 % of the value observed in water flow. The difference progressively increased from that observed at $\lambda = 45$ to the maximum and then decreased to that observed at $\lambda = 0$.

A large increase in T_u was observed in the wake at this and all other Reynolds numbers tested. At $\lambda = 45$ the intensity inside the wake was 42 % greater than that observed in water flow. A maximum was observed at $\lambda = 14$. At this state of degradation, the increase was about 180 % at the centre of the wake. The difference progressively diminished with decreasing λ.

At $x = 1{\cdot}5d$, the turbulence-intensity profiles were relatively closer to those

of tap water. The maximum reduction of T_u outside the wake occurred at $\lambda = 14$. Inside the wake, however, the difference between water and polymer-solution turbulence intensities was greatly diminished, reaching a maximum at $\lambda = 10$, where the difference was about 40 % at the centre of the wake.

The wake width, defined by Bloor (1965) as the point at which high frequency spikes were first observed in the free shear layer as the hot wire or film was moved toward the centre of the wake, was obtained only at $x = 1{\cdot}5d$ for various values of Re and λ. In spite of the difficulty and uncertainty of hot-film measurements in general and of the wake-width measurements in particular, the results presented in figure 22 are sufficiently interesting as far as their relation to other measurements and to the effect of degradation on near-wake flow is concerned. It is apparent that the wake width first decreases with decreasing λ and then returns to its water-like values as $\lambda \to 0$. As an example, at $Re = 12 \times 10^4$, it reduces from $1{\cdot}85d$ at $\lambda = 76$ to $1{\cdot}3d$ at $\lambda = 14$, with a reduction of 30 %.

The microscale of turbulence was measured at $x = 1{\cdot}5d$ for various values of Re and λ. For water, it remained at a relatively constant value of 0·07 ft. At higher values of λ the microscale was found tc be 0·045 ft, and at moderate values of λ it decreased to the minimum value of 0·03 ft. At $\lambda = 14$ it increased to about 0·04 ft. and at $\lambda = 3$ it was found to increase further to approximately 0·05 ft.

The frequency spectrum measurements in the wake revealed nothing additional to those features already noted for wall-pressure frequency spectrum measurements. In general, the polymer-solution flow exhibited r.m.s. values considerably lower than those obtained in water flow. The dominant frequency was also suppressed as λ decreased, with a maximum suppression at $\lambda = 15$. With further degradation, the amplitudes increased, and approached the r.m.s. values obtained for the pure solvent.

The foregoing measurements revealed, in summary, that polymer has profound effects on the near-wake flow; pressures are relatively higher, T_u progressively increases, reaches a maximum and then decreases as $\lambda \to 0$, and the width of the wake is reduced below that observed for solvent flow. The sizes of changes in and outside the wake are dependent upon Re and λ and gradually disappear as $\lambda \to 0$.

3.2.6. *Drag reduction with nearly neutrally buoyant particles.* The results of the extensive direct-drag and pressure distribution measurements, carried out by the senior author, in suspension flows (tap water as the support fluid) are summarized in figure 23. All the data have shown, in the range of sizes and concentrations studied, that (*a*) spherical particles do not appreciably affect the characteristics of the flow in the range $5 \times 10^4 < 2{\cdot}5 \times 10^5$; (*b*) fibres can considerably reduce the drag coefficient (the amount of reduction is strongly dependent upon concentration and possibly upon the fibre elasticity and aspect ratio); (*c*) *neither the spherical particles nor springy fibres cause a* 'drag crisis', i.e. all pressure and drag data exhibit smooth variations with increasing Re and suspension concentration; and finally, (*d*) the results are not dependent on the pump running time (a maximum of 72 h was tried), i.e. the abrasion of particles by friction and collision and the water absorption (very low) of nylon fibres over a period of time have no noticeable effect on the characteristics of the flow.

Quantities such as turbulence intensity, wake width, etc. have not been

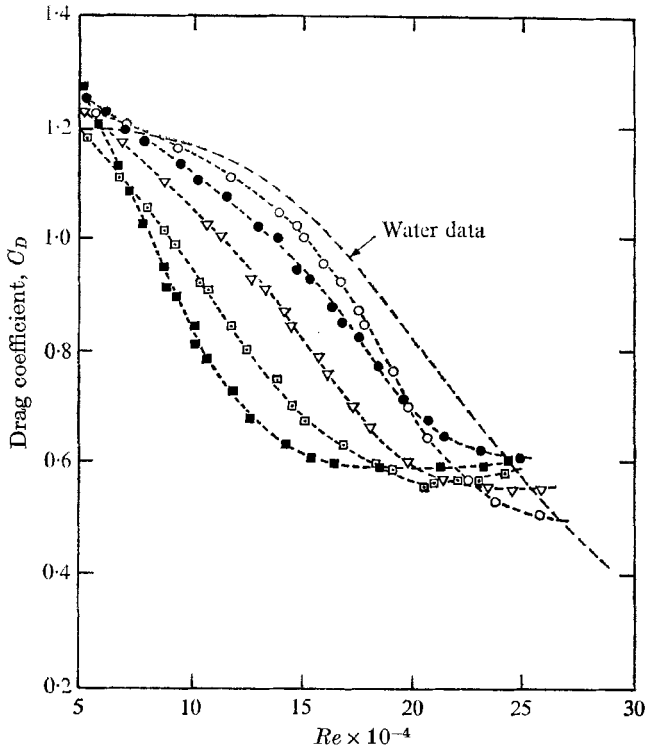

FIGURE 23. Variation of C_D with Re and concentration C for a 1 in. cylinder in suspension flows. With spherical particles: ○, C = 0·01 (by volume); ●, C = 0·04. With fibres (L/d = 100): ▽, C = 0·01; ⊡, C = 0·025; ■, C = 0·04. (Note: water viscosity is used to calculate the Reynolds number since the inter-particle collisions do not dominate the flow for the concentrations and L/d ratios used (Kerekes & Douglas 1972).)

measured for obvious reasons. Suffice it to say that the pressure distribution on the front part of the cylinder remained roughly between laminar and turbulent distributions for water and on the rear half of the cylinder remained higher than that of water and somewhat below that of polymer. At no time did the pressures exhibit large-scale oscillations anywhere on the cylinder in a manner similar to that shown in figure 18. However, a 5 p.p.m. polymer solution degraded in a barrel by rapid stirring to a level of $\lambda = 12$ and introduced into the fibre suspension flow (at a concentration of 1·5 %) caused once again the remarkable 'drag crisis', with all of its attendant consequences, as soon as Re reached a value of $8{\cdot}2 \times 10^4$. This particular avenue of investigation has been carried out only as a matter of curiosity and has not been explored in detail.

4. Discussion of results

First, all the data presented in the previous sections show that for $\lambda > \lambda_c$ the polymer solution yields relatively monotonic changes in C_D, C_p, the wake width, Strouhal frequency, turbulence intensity, etc., in a manner similar to that observed in pure-solvent flows, but at smaller Reynolds numbers. When

λ decreases to a certain value while Re remains smaller than the smallest observed Re_c, the degraded solution begins to lose its effectiveness and the characteristics of flow return to those of the pure solvent in the subcritical state. For $Re > Re_c$, however, the increasing degradation causes a drag crisis at a particular value of λ, nearly independent of concentration and body size. In other words, the addition to polymer (here we have to limit our observations to Polyox WSR-301) to water causes water-like effects to occur at lower Reynolds numbers. In fact, at one Re several regimes of flow can be observed as λ decreases (see figures 14, 15 and 22), i.e. a solvent-like behaviour for large values of λ (fresh solutions), a transitional state for decreasing values of λ, drag crisis at $\lambda \simeq 10$, and finally, return to the solvent-like subcritical state for $\lambda < 10$.

Second, it is evident from the data presented here that the flow with additive about the cylinder precipitates the occurrence of the flow characteristics normally observed at higher Re. In a related observation, the reduced pipe friction coefficients in polymer-solution flows were interpreted by Emerson (1965) as corresponding to those found at much higher Reynolds numbers and this interpretation was used in ship-model tests in matching the Reynolds as well as Froude numbers of the model and the prototype.

Third, the simultaneous reduction of the wake width (figure 22) and C_D (figures 8, 14 and 15) is in conformity with the accepted explanations of the drag decrease with the wake width even if the mechanism with which this reduction with decreasing λ is brought about is not yet clear. However, neither the position of the separation point at small values of λ, nor the variation of the pressure distribution behind the cylinder, nor the apparent increase of turbulence in the near-wake can be easily related to the decrease in C_D or wake width or interpreted in terms of the arguments employed for the flow of Newtonian solvents (see figures 11, 16, 17, 20 and 21). For a 25 p.p.m. solution with $10 < \lambda < 20$, for example (see figure 11(*b*)), the upstream limit of the separation point is nearly identical to that of the pure-solvent flow whereas C_D in the same range (figure 8) is considerably lower than that for the solvent flow, the wake width (figure 22) is considerably reduced and the intensity of turbulence in the near wake is considerably increased. It is tempting to think that the increased mixing (larger T_u) in the wake increases the pressure behind the cylinder (figure 17) and gives rise to the smaller C_D measured, but this argument does not explain the reasons leading to the increase of T_u behind the cylinder. The foregoing arguments rather lead to the conclusion that the position of the separation point, T_u and C_p are not related in a simple manner and that, as has already been argued by Luikov *et al.* (1969), the earlier drop in drag caused by the polymer cannot simply be ascribed to the contraction of the wake or to an earlier onset of turbulent separation. The additives (polymer of fibres) must have profound effects on free shear layers and in particular on the vortex formation, growth and motion behind bluff bodies with or without fixed separation points (exploratory experiments with a flat plate normal to the flow are described in Sarpkaya & Rainey (1971) and the strong destabilizing effect of the additive on the phenomenon known as the vortex breakdown is described in Sarpkaya (1970)).

Finally, the results show that C_D–Re relationship in the transition region may

be affected by fibres suspended in the pure solvent, that spherical particles, at comparable concentrations, have very little influence on transition and that neither the spherical particles nor fibres cause a drag crisis.

The foregoing results suggest that (*a*) the rotation of particles is an essential part of the drag-reduction mechanism (such a motion may be seen to correspond to a maximum dissipation of viscous energy (Cox & Mason 1971)); (*b*) the possible attachment to polymer chains by adsorption to the cylinder surface is neither sufficient nor necessary (contrary to the previous arguments by Sarpkaya *et al.* 1972) for the interpretation of the results; (*c*) the possible existence of an additive-concentration layer near the cylinder wall (Rivard & Kulinski 1972) is not sufficient to explain the drag crisis; (*d*) one or more additional characteristics of the dissolved polymer (such as entanglement or aggregation of the polymer molecules, their deformation and rotation under the stresses exerted on them, deformation history, etc.) must be responsible for the drag crisis in non-cavitating flows; and finally, (*e*) the drag-reduction mechanism should be based on a non-elastic and non-continuum medium in which the visco–inertial action of the particles interacts with the surrounding fluid.

5. Concluding remarks

The reference measurements of drag, pressure, Strouhal frequency, etc., in water showed good agreement with previous data obtained principally in air and provided the necessary basis for comparison to the corresponding polymer-solution data.

The results did not lead to a complete understanding of the causes of drag reduction in bluff-body flows but revealed a number of new facts. (*a*) Separation-line instability observed by Brennen (1970) in cavitating flows in the subcritical flow regime can also occur in non-cavitating flows but in the critical flow regime. (*b*) The mechanical degradation of the polymer has profound effects on all features of flow particularly in the critical flow regime. It precipitates the occurrence of the flow characteristics normally observed at higher Reynolds numbers and can lead to drag crisis (large oscillations in pressure, sudden drop in drag, sudden loss of dominant frequency, etc.). (*c*) Polymer solutions, at all levels of degradation, as well as particle suspensions, give rise to relatively larger pressures on the rear half of the cylinder and consequently to smaller drag coefficients. (*d*) The shift of the separation point, narrowing of the wake, rise of base pressure, rise of the turbulence intensity in the near wake and reduction of drag do not appear to be related by a simple mechanism. (*e*) The measurements of turbulence intensity show that the earlier transition and drag crisis cannot be ascribed to a change in free-stream turbulence. (*f*) The presence of instabilities in the boundary layer near separation, even in highly degraded solutions and Brennen's (1970) and Brennen & Gadd's (1967) experiments, just to name a few, strengthen the view that the viscoelastic manifestations of fresh solutions may only be a side effect of their drag-reducing and instability promoting properties.

The results and data presented here support one of the earlier concepts developed to explain the friction reduction in pipes (e.g. Lumley 1969; Barenblatt

1969; Ellis, Ting & Nadolink 1972; Forame, Hansen & Little 1972) that the entanglement or aggregation of polymer molecules, their deformation, rotation and translation under the stresses exerted on them, and the deformation history could be one of the most important mechanisms involved in drag reduction, separation-line instability, drag crisis, etc. If correct, such a concept requires the development of appropriate constitutive equations for a non-elastic and non-continuum medium in which the visco–inertial action of the particles interact in a complex manner with the surrounding fluid motion. Additional studies with other types of bodies, polymer solutions, and suspensions of relatively long elastomer filaments, which can entangle and form very complicated coils, may shed further light to the understanding of the phenomenon.

The senior author is indebted to the Aerodynamische Versuchsanstalt-Göttingen of DFVLR and especially to its director Prof. H. Schlichting for their hospitality during his sabbatical year in Göttingen, where part of this investigation has been carried out. The work was sponsored by the Naval Ship Systems Command General Hydromechanics Research Program, administered by the Naval Ship Research and Development Center. We wish to thank the reviewers for their constructive comments on the first draft of this paper, Dr J. W. Hoyt for an advance copy of his Freeman Award Review of "The Effect of Additives on Fluid Friction" (1972), and Dr T. M. Houlihan and Mr T. F. Christian for their assistance with the hot-film measurements.

REFERENCES

ACHENBACH, E. 1971 *J. Fluid Mech.* **46**, 321.

AKAD, D. 1969 M.S. thesis, Naval Postgraduate School, Monterey.

BARENBLATT, G. I. 1969 *Heat Trans. Soviet Res.* **1**, 102.

BARENBLATT, G. I., BULINA, I. G. & MYASNIKOV, V. P. 1965 *Zh. Prikl. Mekh. i. Tekhn. Fiz.* **3**, 95.

BATCHELOR, G. K. 1967 *An Introduction to Fluid Dynamics*. Cambridge University Press.

BEARMAN, P. W. 1969 *J. Fluid Mech.* **37**, 577.

BLOOR, M. S. 1965 *J. Fluid Mech.* **19**, 290.

BRENNEN, C. 1970 *J. Fluid Mech.* **44**, 51.

BRENNEN, C. & GADD, G. E. 1967 *Nature*, **215**, 1368.

BRYSON, A. W., ARUNACHALAM, V. R. & FULFORDS, G. D. 1971 *J. Fluid Mech.* **47**, 209.

BUBLITZ, P. 1971 *A.V.A. (Göttingen) Rep.* 71-J-11.

CHENARD, J. H. 1967 M.S. thesis, Naval Postgraduate School, Monterey.

COX, R. G. & MASON, S. G. 1971 In *Annual Reviews of Fluid Mechanics*, vol. 3, p. 291. Annual Reviews Inc.

CRAWFORD, H. R. & PRUITT, G. T. 1963 In *Proc. Symp. on Non-Newtonian Fluid Mechanics*, 56th Annual Meeting, Inst. Chem. Eng., Houston, Texas.

DELANEY, N. & SORENSEN, N. 1953 *N.A.C.A. Tech. Note*, no. 3038.

DRESCHER, H. 1956 *Z. Flugwiss.* **4**, 17.

ELLIS, A. T., TING, R. Y. & NADOLINK, R. H. 1972 *J. Hydronautics*, **6**, 66.

EMERSON, A. 1965 *Trans. N.E. Coast Inst. Engrs & Shipbuilders*, **81**, 201.

FAGE, A. & WARSAP, A. 1930 *Aero. Res. Counc. R. & M.* no. 283.

FLORY, P. J. 1953 *Principles of Polymer Chemistry*. Cornell University Press.

FORAME, P. C., HANSEN, R. J. & LITTLE, R. C. 1972 *A.I.Ch.E. J.* **18**, 213.

FUNG, Y. C. 1960 *J. Aero. Sci.* **27**, 801.

GADD, G. E. 1966 *Nature*, **211**, 1969.

GOLDSTEIN, S. 1965 *Modern Developments in Fluid Dynamics*, vol. 2. Dover.

HAYES, M. F. 1966 M.S. thesis, Naval Postgraduate School, Monterey.

HENDRICKS, R. K. 1970 M.S. thesis, Naval Postgraduate School, Monterey.

HINZE, J. O. 1959 *Turbulence*. McGraw-Hill.

HOYT, J. W. 1965 In *A.S.M.E. Symposium on Rheology* (ed. by A. W. Morris), p. 71.

HOYT, J. W. 1968 In *Solution Properties of Natural Polymers*, p. 207. London: Chemical Society.

HOYT, J. W. 1972 *J. Basic Engng, A.S.M.E.* **94**, 258.

HUMPHREYS, J. S. 1960 *J. Fluid Mech.* **9**, 603.

JAMES, D. F. 1967 Ph.D. thesis, California Institute of Technology.

JAMES, D. F. & ACOSTA, A. J. 1970 *J. Fluid Mech.* **42**, 269.

JONES, G. W., CINCOTTA, J. J. & WALKER, R. W. 1969 *N.A.S.A. Tech. Rep.* R-300.

KALASHNIKOV, V. N. & KUDIN, A. M. 1970 *Nature*, **225**, 445.

KELL, R. E. 1971 M.S. thesis, Naval Postgraduate School, Monterey.

KEREKES, R. J. E. & DOUGLAS, W. J. M. 1972 *Can. J. Chem. Eng.* **50**, 325.

KLEBANOFF, P. S. & TIDSTROM, K. D. 1972 *Phys. Fluids*, **15**, 1173.

LANG, T. G. & PATRICK, H. V. L. 1967 *Naval Ordnance Test Station Rep.* TR-4379. (See also *A.S.M.E. Paper*, 66-WA/FE-33.)

LIENHARD, J. H. 1966 *Washington State University Bull.* no. 300.

LUIKOV, A. V., SHULMAN, Z. P. & PURIS, B. I. 1969 *Heat Trans. Soviet Res.* **1**, 121.

LUMLEY, J. L. 1969 In *Annual Reviews of Fluid Mechanics*, vol. 1, p. 367. Annual Reviews Inc.

MCCLANAHAN, T. & RIDGELY, P. J. 1968 M.S. thesis, Naval Postgraduate School, Monterey.

MCGREGOR, D. 1957 *University of Toronto Inst. Aerophys. Tech. Note*, no. 14.

MAIR, W. A. & MAULL, D. J. 1971 *J. Fluid Mech.* **45**, 209.

MASKELL, E. C. 1965 *Aero. Res. Counc. Rep.* no. 3400.

MERRILL, E. W., SMITH, K. A. & CHUNG, R. Y. C. 1966 *A.I.Ch.E. J.* **12**, 809.

MERRILL, E. W., SMITH, K. A., SHIN, H. & MICKLEY, H. S. 1966 *Trans. Soc. Rheology*, **10**, 335.

PATERSON, R. W. & ABERNATHY, F. H. 1970 *J. Fluid Mech.* **43**, 689.

POPE, A. & HARPER, T. 1966 *Low-speed Wind Tunnel Testing*. Wiley.

POPOV, S. G. 1966 *Fluid Dyn.* **1**, 107.

RIVARD, W. C. & KULINSKI, E. S. 1972 *Phys. Fluids*, **15**, 728.

ROSHKO, A. 1961 *J. Fluid Mech.* **10**, 345.

RUSCZYCKY, M. A. 1965 *Nature*, **206**, 614.

SANDERS, J. V. 1967 *Int. Shipbldg Prog.* **14**, 140.

SARPKAYA, T. 1970 *Naval Postgrad. School Monterey Rep.* NPS-59SL0071A.

SARPKAYA, T. 1971 *J. Fluid Mech.* **45**, 545.

SARPKAYA, T. & RAINEY, P. G. 1971 *Naval Postgrad. School Monterey Rep.* NPS-59SL 1021A.

SARPKAYA, T., RAINEY, P. G. & KELL, R. E. 1972 *Naval Postgrad. School Monterey Rep.* NPS-59SL72072A

SCHIMMELS, J. N. 1971 M.S. thesis, Naval Postgraduate School, Monterey.

SCHLICHTING, H. 1968 *Boundary Layer Theory*, 6th edn. McGraw-Hill.

TANI, I. 1964 In *Progress in Aeronautical Sciences* **5**, 70.

VIRK, P. S. 1971 *J. Fluid Mech.* **45**, 417.

WHITE, A. 1966 *Nature*, **211**, 1390.

WHITE, A. 1967 *Nature*, **216**, 994.

WHITE, D. A. 1966 *Nature*, **215**, 277.

WHITE, W. C. & MCELIGOT, D. M. 1969 *A.S.M.E. Paper*, 69–WA/FE-20.